NASA Contractor Report 194458

Numerical Simulation of Cylindrical, Self-Field MPD Thrusters With Multiple Propellants

Michael R. LaPointe
Sverdrup Technology, Inc.
Lewis Research Center Group
Brook Park, Ohio

Prepared for
Lewis Research Center
Under Contract NAS3-25266

NASA
National Aeronautics and
Space Administration

Numerical Simulation of Cylindrical, Self-Field MPD Thrusters With Multiple Propellants

Michael R. LaPointe
Sverdrup Technology, Inc.
Lewis Research Center Group
Brook Park, Ohio 44142

ABSTRACT

A two-dimensional, two-temperature, single fluid MHD code was used to predict the performance of cylindrical, self-field MPD thrusters operated with argon, lithium, and hydrogen propellants. A thruster stability equation was determined relating maximum stable $J^2/\dot{m}$ values to cylindrical thruster geometry and propellant species. The maximum value of $J^2/\dot{m}$ was found to scale as the inverse of the propellant molecular weight to the 0.57 power, in rough agreement with limited experimental data which scales as the inverse square root of the propellant molecular weight. A general equation which relates total thrust to electromagnetic thrust, propellant molecular weight, and $J^2/\dot{m}$ was determined using reported thrust values for argon and hydrogen and calculated thrust values for lithium. In addition to argon, lithium, and hydrogen, the equation accurately predicted thrust for ammonia at sufficiently high $J^2/\dot{m}$ values. A simple algorithm is suggested to aid in the preliminary design of cylindrical, self-field MPD thrusters. A brief example is presented to illustrate the use of the algorithm in the design of a low power MPD thruster.

NOMENCLATURE

I_{sp}	specific impulse (s)
J	discharge current (A)
La	anode length (m, unless noted)
Lc	cathode length (m, unless noted)
$\dot{m}$	mass flow rate (kg/s)
M_{Ar}	argon molecular weight (39.95 amu)
M_{pr}	propellant molecular weight (amu)
MPDT	magnetoplasmadynamic thruster
P_{dis}	power to dissociate propellant (W)
P_{ion}	power to fully ionize propellant (W)
P_{pl}	power available in plasma (W)
P_{TOT}	total discharge power (W)
Ra	anode radius (m, unless noted)
Rc	cathode radius (m, unless noted)
T	thrust (N)
T_{EM}	electromagnetic thrust (N)
V	total thruster voltage (V)
V_{pl}	plasma voltage (V)
α	electromagnetic thrust parameter ($0 \le \alpha \le 3/4$)
μ_0	permeability of free space ($4\pi \times 10^{-7}$ H/m)
η_f	thruster flow efficiency
η_{tot}	total thruster efficiency
X_{dis}	dissociation potential (eV)
X_{ion}	ionization potential (eV)

I. Introduction

The magnetoplasmadynamic (MPD) thruster is an electric propulsion device which has been advocated for a variety of mission applications, ranging from low power orbit raising maneuvers to robotic and piloted multi-megawatt planetary expeditions.[1-3] In its basic form, the MPD thruster consists of a central cathode and concentric anode (Figure 1). An electric discharge is ignited between the electrodes, and ionizes a gas propellant injected through an insulating backplate. The interaction of the electric arc current with the self-induced magnetic field accelerates the resulting plasma to produce thrust. Steady-state MPD thrusters have been operated at power levels approaching 600 kW_e, while pulsed, quasi-steady devices have been operated in the multi-megawatt power range.[4,5] The engine is designed to provide low, continuous thrust with specific impulse (I_{sp}) values of 1,000 to 10,000 s, with the higher I_{sp} values corresponding to the use of low molecular weight propellants.[4,5] The ability to scale MPD thrusters in size, power, and performance allows an evolutionary approach to MPD propulsion technology, paced by the development of space power systems and prevailing mission architectures.

Although simple in design and robust in operation, MPD thruster performance has typically been limited by low thrust efficiency in regimes of interest.[5]

*Senior engineer, member AIAA

Applied magnetic fields[5,6] and flared electrode geometries[7,8] have been shown to improve MPD thruster efficiency and specific impulse, but for reasons poorly understood at present. Severe electrode erosion has been observed at high values of specific impulse, and corresponds to the onset of significant discharge voltage oscillations and unsteady thruster operation. Several mechanisms have been proposed to explain the onset of MPD thruster instabilities, including anode mass starvation[9], flow choking due to enhance back electromotive forces,[10,11] and the triggering of electrothermal and gradient driven instabilities as the plasma approaches full ionization.[12,13] Different operating conditions may trigger one or more of the proposed mechanisms, significantly limiting thruster lifetime and performance. In addition, the occurrence of plasma microinstabilities has been predicted[14] and experimentally observed[15] in MPD thrusters over a range of operating conditions. The presence of microturbulence may enhance the plasma resistivity, resulting in anomalous energy dissipation and a reduction in thruster efficiency.

Although applied magnetic fields improve thruster specific impulse and efficiency, recent extended-wear tests of a 60 kW_e applied-field MPD thruster uncovered significant anode sputtering by the argon propellant.[16] The sputter erosion mechanism becomes important when the propellant energy exceeds the sputter threshold for the anode material. As noted by Mantenieks and Myers,[16] the sputter yield of metals do not vary significantly over a range of similar energies, hence it may not be possible to eliminate the sputter mass loss in an applied-field MPD thruster through the use of alternate anode materials. An alternate approach is to use light propellants such as hydrogen, deuterium, or lithium, which have low sputter yields at the energies of interest.[16] The higher specific impulse and thrust efficiencies associated with the use of low molecular weight propellants, coupled with the extensive anode sputtering encumbered by heavy-ion propellants, provides an impetus to evaluate self-field MPD thrusters operated with hydrogen and lithium propellants.

Numerical Simulations.

A steady-state, two-dimensional code has been developed at the National Aeronautics and Space Administration (NASA) Lewis Research Center to predict self-field MPD thruster performance.[17-19] The numerical simulation is based upon a fully ionized, single fluid approximation to the MHD equations, and includes viscous forces, classical plasma transport, and Hall effects. Maxwell's equations and a generalized Ohm's law are used to couple the electromagnetic equations to the fluid equations. A single temperature version of the model was previously used to predict thrust, plasma voltage, and flow efficiency for straight and flared cylindrical electrode geometries, assuming a fully-ionized argon propellant.[17] Thrust predictions were in good agreement with experimentally determined values. Although voltage-current predictions followed experimentally observed trends, the model does not incorporate electrode falls or microturbulent plasma processes, and the calculated plasma voltage drops were significantly lower than the experimentally measured total discharge voltages.

A two-temperature version of the code employing separate electron and ion energy equations[18] was used to predict the performance of a matrix of cylindrical self-field thruster geometries over a range of operating conditions, again assuming a fully ionized argon propellant. Results of the two-temperature simulations indicated that shorter electrode lengths enhanced stable thruster operation at high values of specific impulse, while longer electrode lengths were required to improve thruster flow efficiency at lower values of specific impulse. The specific impulse for a self-field MPD thruster is related to $J^2/\dot{m}$, a parameter often used to characterize MPD thruster performance.[5] High values of $J^2/\dot{m}$ correspond to predominantly electromagnetic acceleration and high values of specific impulse, while low values of $J^2/\dot{m}$ correspond to predominantly electrothermal acceleration and lower values of specific impulse.

The two-temperature simulations did not converge for certain combinations of geometry and $J^2/\dot{m}$, with numerical oscillations appearing in both the fluid variables and the electromagnetic field quantities. Because the code is based upon a steady-state formulation, it is not clear whether the oscillations result from initial perturbations in the fluid variables or in the field variables, but the effect is most apparent in values of the fluid density and temperature near the cathode tip and in the radial electric field distribution between the electrodes. Oscillations in these variables affect the fluid pressure and flow velocity, the induced magnetic field distribution, the plasma voltage, and the plasma transport coefficients. The simulation does not in general terminate with a catastrophic numerical instability, but the coupled oscillations in the fluid and field variables prevent the code from converging for

specific combinations of thruster geometry and $J^2/\dot{m}$ values.

Based upon the numerical convergence of the two-temperature code, an equation was formulated which relates the maximum stable value of $J^2/\dot{m}$ to the simulated cylindrical thruster geometries:

$$\frac{J^2}{\dot{m}} \leq \frac{6.25 \times 10^9}{Rc}\left(\frac{Lc}{La}\right)\left[5 - \left(\frac{La}{Ra}\right) + 4\left(\frac{10*Rc-Ra}{2.5}\right)\right] \frac{A^2\text{-}s}{kg} \quad (1)$$

where J is the discharge current in amps, $\dot{m}$ is the argon propellant mass flow rate in kg/s, and Ra, La, Rc, and Lc are the anode radius and length and cathode radius and length, respectively, measured in cm. The validity of Equation 1 is limited to straight cylindrical electrode geometries with $Rc \geq 0.5$ cm, $Ra \geq 2.5$ cm, $5 \leq Ra/Rc \leq 10$, $La/Ra \leq 5$, and approximately equal electrode lengths ($La \approx Lc$), and assumes uniform propellant injection at the backplate. The onset of MPD thruster voltage oscillations with increasing $J^2/\dot{m}$ has been extensively documented, and a comprehensive data base listing maximum $J^2/\dot{m}$ values for a variety of cylindrical self-field MPD thrusters has been compiled by Preble.[20] The maximum stable $J^2/\dot{m}$ values predicted by Equation 1 were compared to experimental values of $J^2/\dot{m}$ at onset for thruster geometries in Preble's data set which satisfied the constraints associated with Equation 1. The predicted onset values were within 20% of the experimentally observed values,[18] indicating that Equation 1 could be used to estimate maximum $J^2/\dot{m}$ values for cylindrical, self-field thrusters operated with argon propellant, subject to the geometric constraints outlined above.

An additional constraint recently incorporated into the NASA LeRC MPD thruster model defines the minimum cylindrical cathode surface area required to support a given thruster discharge current via thermionic emission.[19] To sustain cathode integrity over the thousands of hours required for typical low thrust mission profiles, the cathode temperature should be limited to values below approximately 1470 K.[21] The corresponding current densities for impregnated tungsten rod cathodes lies between 10-20 A/cm^2, the latter value used by Myers et al.[22] to design a rod cathode suitable for megawatt MPD thruster applications. For a given discharge current, and assuming uniform thermionic emission from the cathode surface, the minimum required cathode surface area is simply the discharge current divided by the emission current density. For a given cathode radius, the minimum surface area requirement determines a minimum cathode length for use in the numerical simulations. Incorporating the cathode emission constraints in the numerical model, it was shown that long-life, cylindrical self-field MPD thrusters operated with argon propellants would probably not be able to provide the necessary combination of specific impulse, efficiency, and lifetime required for missions of interest.

With numerical results predicting inadequate self-field thruster performance, and experimental results demonstrating excessive applied-field MPD thruster anode erosion,[16] argon can no longer be considered an attractive propellant for flight-qualified MPD thrusters. As a first step toward modeling the performance of lower molecular weight propellants, the self-field MPD thruster code described above was used without modification to predict the performance of hydrogen and lithium propellants. For purposes of this preliminary investigation all propellants were assumed to be fully dissociated and ionized.

In the following section, numerical predictions are compared with experimental results to estimate the accuracy of the simplified model approximations discussed above. In Section III, the model is used to simulate a 100-kW_e class cylindrical self-field MPD thruster operated with argon, hydrogen, and lithium propellants over a range of $J^2/\dot{m}$ values. The numerical results are used to evaluate the effect of propellant species on stable thruster operation, leading to a modified expression for Equation 1. Numerical simulations and experimental thrust data are then combined to generate analytic expressions relating total thrust to $J^2/\dot{m}$ and propellant molecular weight. In Section IV the modified stability equation and the analytic thrust expressions are combined into a simple algorithm to predict the performance of cylindrical, self-field MPD thrusters. An example is given outlining the utility of the algorithm, and the paper concludes with some final remarks in Section V.

II. Comparison With Experiment

The two-temperature self-field MPD thruster simulation was tested against the experimental performance of the Princeton University full-scale benchmark thruster (FSBT) and the Osaka University MY-I thruster, both of which have been operated with

hydrogen propellants. No comparisons between model and experiment were possible for lithium, as thrust data has only been reported for applied-field lithium-fed MPD thrusters.[23] Although this is a disadvantage in assessing the reliability of the self-field model results, hydrogen is perhaps the more difficult propellant for the simplified code to model because molecular dissociation and full ionization are assumed throughout. The dissociation potential for diatomic hydrogen is 2.26 eV, with a first ionization potential of 13.6 eV. The dissociation and first ionization potentials for lithium are approximately 1.12 eV and 5.39 eV, respectively. Argon, with a first ionization potential of 15.76 eV, is a monopropellant, and dissociation effects may be legitimately excluded. Randolph[24] has shown experimentally that argon is sufficiently ionized even at low discharge currents for the full ionization approximation to be valid, and previous simulations[17-19] assuming fully-ionized argon have provided accurate thrust predictions for a variety of thruster geometries. Unlike argon, there is no assurance that the full ionization approximation will be valid for either lithium or hydrogen under the operating conditions of interest. Using energy balance arguments, Myers[25] estimated an upper bound of approximately 10% for hydrogen ionization in 100-kW class applied-field MPD thrusters. However, fractional ionization of even a few percent is usually sufficient for the classical plasma transport coefficients to be accurately modeled with a full ionization approximation,[26] and it is not expected that global performance parameters such as thrust and plasma voltage will differ significantly from the values which would be obtained using a more exact simulation. Code predictions are compared below with experimental data for the Princeton University full-scale benchmark thruster operated with argon and hydrogen propellants, and the Osaka University MY-I thruster operated with hydrogen, to assess the accuracy of the two-temperature, fully-ionized model approximations.

Princeton FSBT Comparisons: Argon

The FSBT, depicted schematically in Figure 2, is a pulsed, quasi-steady device which consists of an insulated, cylindrical discharge chamber with an inner radius of approximately 6.1 cm and a total chamber depth of 6 cm. An annular aluminum anode is set flush against the discharge chamber exit plane, with an inner radius of approximately 5 cm and a length of 1 cm. A 0.95 cm radius, 10 cm long 2%-thoriated tungsten rod cathode protrudes from a boron nitride insulating backplate, and extends roughly 4 cm downstream of the anode exit plane. Propellant is injected at the backplate through an annular slit at the base of the cathode and through 12 evenly spaced holes distributed azimuthally at a fixed radius in the boron nitride backplate. The FSBT is mounted on a horizontal, free-swinging pendulum arm thrust stand, with thrust measured by a position transducer. Thrust stand calibration procedures and data acquisition systems are discussed in detail by Gilland.[27]

The full-scale benchmark thruster has been extensively tested with argon propellant.[27,28] Figure 3 presents a compilation of experimental thrust values reported for the standard FSBT geometry, operated over a range of discharge currents with an argon mass flow rate of 6 g/s. Also displayed on the figure are numerical thrust predictions based on the two-temperature model, assuming full ionization and uniform propellant injection at the backplate. Both electromagnetic thrust and total thrust are accurately predicted by the model up to a discharge current of 22 kA, corresponding to a $J^2/\dot{m}$ value of 8×10^{10} A^2-s/kg. Above this value the two-temperature code no longer converges. Based on the previous modeling results, it is expected that the numerical oscillations coincide with the onset of instabilities in the actual FSBT thruster, and indeed the experimentally determined value of onset occurs at a $J^2/\dot{m}$ value of approximately 7.5×10^{10} A^2-s/kg, in good agreement with the numerical simulation.

Figure 4 displays the experimentally measured total voltage and the predicted plasma voltage as a function of discharge current. The general voltage-current trend is reproduced, but the magnitude of the predicted voltage falls below the total measured voltage due to a lack of electrode fall potentials in the model. Nevertheless, the ability to accurately calculate the thrust, predict the onset of instability, and reproduce the general voltage-current trends for the FSBT with argon propellant extends a measure of confidence to the numerical simulation results which follow.

Princeton FSBT Comparisons: Hydrogen

The full-scale benchmark thruster has recently been operated with 1 g/s of hydrogen[28,29] for discharge currents exceeding 21 kA, corresponding to $J^2/\dot{m}$ values in excess of 4.5×10^{11} A^2-s/kg. Figure 5 shows the measured and predicted values for the electromagnetic thrust and the total thrust as a function of discharge current. The numerical

predictions of electromagnetic thrust are accurate over the range of simulated discharge currents, but the two-temperature model begins to underpredict the total thrust for discharge currents exceeding 12 kA. The simulation does not converge for discharge currents exceeding 15 kA, as noted by the range of oscillatory simulated thrust values denoted in the figure. Because the model retains several simplifying assumptions, it is possible (perhaps probable) that the present version of the code is inadequate to allow accurate predictions of thruster performance with hydrogen at the higher discharge currents. However, it should be noted that significant voltage hash was observed in the experiments for discharge currents as low as 4 kA, suggesting that perhaps the thruster was not operating in an optimally stable regime. In addition, some evidence of insulator erosion was apparent after several firings, though no effort was made to quantify the erosion loss during these initial test discharges.[30] Consequently, some insulator material could be contributing to the propellant mass flow, resulting in a higher measured thrust value. Although the discrepancy between prediction and measurement may be a result of the model approximations, the preliminary performance data reported for the FSBT operated with hydrogen are consistent with operation above the onset of significant voltage oscillations indicative of thruster instabilities. Refinements to the model and additional experimental testing of the FSBT with hydrogen should be performed to resolve these issues.

The plasma voltages predicted by the model are compared with the averaged experimental discharge voltages in Figure 6, and for the stable numerical range of operating values the predicted plasma voltage trends agree with the trends in the experimentally measured total voltage, within a nearly constant voltage offset. As before, this voltage difference is presumably due to the lack of electrode fall potentials in the model. The total thruster efficiency, defined as:

$$\eta_{tot} = \frac{T^2}{2\,\dot{m}\,V\,J} \qquad (2)$$

may be calculated from the thrust data in Figure 5 and the total voltage data in Figure 6. The thruster efficiency exceeds 50% at discharge currents above 18 kA ($J^2/\dot{m} \geq 3.2\times10^{11}$ A^2-s/kg), and approaches 70% for discharge currents above 20 kA ($J^2/\dot{m} \geq 4\times10^{11}$ A^2-s/kg). By comparison, the highest thruster efficiency for argon, obtained using Figures 3 and 4, approaches a maximum value of 17% at 22 kA ($J^2/\dot{m} = 8\times10^{10}$ A^2-s/kg). These preliminary results indicate that a substantial improvement in thruster performance can be obtained by operating with hydrogen, although a cautionary note must again be raised concerning the issue of stable thruster operation at high $J^2/\dot{m}$ values. The numerical simulation predicts stable FSBT operation with hydrogen for $J^2/\dot{m}$ values below 1.6×10^{11} A^2-s/kg, which corresponds to a maximum thruster efficiency of around 20% for stable operation. Higher $J^2/\dot{m}$ values are predicted to correspond with unstable thruster operation, and the increase in measured thrust and associated thruster efficiency may be due to erosion and entrainment of insulator material. Although some insulator erosion undoubtedly occurs with argon propellant as well, the entrainment of eroded material is arguably more significant at the lower mass flow rates associated with hydrogen. The ability of the two-temperature code to predict the stable regimes of FSBT operation with argon, combined with the experimental evidence of insulator erosion and the observed voltage oscillations during operation with hydrogen, suggest that the preliminary FSBT hydrogen performance data, while encouraging, must be carefully examined at the higher $J^2/\dot{m}$ values.

Osaka MY-I Comparisons: Hydrogen

The Osaka University MY-I thruster,[31] shown schematically in Figure 7, is a quasi-steady, straight cylindrical device with a 5 cm diameter copper anode surrounding a 0.95 cm thoriated tungsten rod cathode. The anode and cathode lengths are 7.5 cm and 4.5 cm, respectively. The thruster is mounted on a thrust stand whose position is measured by a linear differential transformer. Thrust stand calibrations were performed using a small steel ball to provide a measurable impulse while the tank was at atmospheric pressure. Electromagnetic and total thrust values for hydrogen were reported for a mass flow rate of 1.37 g/s and discharge currents up to 20 kA, corresponding to $J^2/\dot{m}$ values up to 290 A^2-s/kg. No information was provided on thruster stability limits or component wear.

Figure 8 shows predicted and measured[31] thrust values for the MY-I thruster as a function of discharge current. The simulation accurately predicts both electromagnetic thrust and total thrust over the range of discharge currents, up to approximately 17 kA ($J^2/\dot{m} = 2.1\times10^{11}$ A^2-s/kg). The code underpredicts the total thrust by almost 20% at 18.5 kA ($J^2/\dot{m}$ =

$2.5x10^{11}$ A^2-s/kg), the highest discharge current modeled for the MY-I thruster geometry. As with the FSBT simulations, the discrepancy at high $J^2/\dot{m}$ values could be an artifact of the simplified approximations inherent in the two-temperature code, or it could be a result of eroded thruster material surreptitiously contributing to the accelerated mass flow. The simulation converged smoothly over the range of discharge currents presented in Figure 8, indicating that the thruster was probably operating below onset. However, without thruster erosion data, it remains unclear whether the low thrust predictions at the highest reported discharge currents are an artifact of the code or represent the entrainment of eroded material, leading to artificially high thrust measurements. Voltage-current characteristics were not provided for the MY-I thruster under the given operating conditions, and a comparison of predicted plasma voltage trends to discharge voltage-current characteristics could not be performed. Reported total thruster efficiencies varied from roughly 6% at the low discharge currents to a maximum of around 35% at 18.5 kA.

In summary, the two-temperature simulation was able to accurately predict the thrust and reproduce general voltage-current trends for the full-scale benchmark thruster operated with argon for $J^2/\dot{m}$ values below onset. The model successfully predicted thrust for the FSBT operated with hydrogen up to $J^2/\dot{m}$ values of $1.4x10^{11}$ A^2-s/kg, but underpredicted the thrust at higher values and did not converge for $J^2/\dot{m}$ values exceeding $2.2x10^{11}$ A^2-s/kg. The discrepancy between experiment and simulation could be due to the simplifying assumptions associated with the fully-ionized, two-temperature model. However, experimental evidence of FSBT insulator erosion and the significant voltage hash measured during operation with hydrogen indicates the thruster may not have been operating stably, and the discrepancies in thrust may be due to the erosion and entrainment of insulator material. The simulation was able to accurately predict the total thrust over a larger range of $J^2/\dot{m}$ values for the MY-I thruster than was possible for the FSBT operated with hydrogen. The model underpredicted the total thrust by roughly 20% at the highest reported $J^2/\dot{m}$ value, which again could be a result of the model approximations or a symptom of thruster erosion and mass entrainment at high $J^2/\dot{m}$. These results suggest that, in addition to model refinements, a serious effort should be made to quantify the erosion and entrainment of thruster material, particularly at the low mass flow rates associated with the low molecular weight propellants.

III. 100 kW_e-class MPDT Simulation

Although the experimental comparisons discussed in the previous section were not entirely satisfactory, the two-temperature model was deemed sufficient for a preliminary study of propellant species effects in a cylindrical, self-field, 100 kW_e-class MPD thruster. A typical discharge current for a 100 Kw_e self-field device is on the order of a few thousand amps, and a constant discharge current of 2500 A was chosen for purposes of the simulation. Variations in the mass flow rate allowed a variety of $J^2/\dot{m}$ values to be simulated, ranging from $2.5x10^{10}$ A^2-s/kg (predominantly electrothermal acceleration) to $5x10^{11}$ A^2-s/kg (predominantly electromagnetic acceleration). A cathode emission current density of 20 A/cm^2 was chosen as a representative value suitable for extended cathode operation. The prescribed discharge current and presumed cathode emission current density set the minimum cylindrical cathode surface area for use in the simulations. A parametric evaluation of Equation 1 indicated that a 2 cm radius, 10 cm long cathode with a 10 cm radius, 10 cm long anode would provide the maximum stable $J^2/\dot{m}$ value for thruster operation with argon at a discharge current of 2500 A, and this geometry was chosen as a baseline to investigate the effects of propellant species on thruster performance.

Propellant Species Effects

The two-temperature MPDT model was operated with argon, lithium, and hydrogen propellants to evaluate the effect of propellant species on the 100 kW_e-class self-field thruster performance. As discussed earlier, propellant dissociation and full ionization were assumed throughout the study. Table 1 and Figures 9 - 12 display the calculated thrust, specific impulse, plasma potential, and flow efficiency, respectively, for a constant discharge current of 2500 A for the various propellants over a range of J^2/m values.

The model converged when simulating thruster operation with argon at $J^2/\dot{m} = 5.0x10^{10}$ A^2-s/kg, but did not converge at $J^2/\dot{m} = 7.5x10^{10}$ A^2-s/kg, indicating that onset occurs between those two operating conditions. Equation 1 predicts a maximum stable $J^2/\dot{m}$ value of $6.3x10^{10}$ A^2-s/kg for the prescribed thruster geometry operated with argon. Additional numerical simulations confirmed that the model converged for $J^2/\dot{m}=6.25x10^{10}$ A^2-s/kg, but not for $J^2/\dot{m}=6.5x10^{10}$ A^2-s/kg, in good agreement with the analytic stability prediction. Code convergence was obtained with lithium at $J^2/\dot{m}=1.75x10^{11}$ A^2-s/kg, but not at $2.0x10^{11}$ A^2-s/kg, indicating that the maximum

stable $J^2/\dot{m}$ value for the thruster operating with lithium is approximately 3 times higher than the maximum stable operating condition obtained with argon. The model converged for $J^2/\dot{m}$ values up to 5.0×10^{11} A^2-s/kg when simulating hydrogen, but did not converge at 5.5×10^{11} A^2-s/kg, indicating that the maximum stable $J^2/\dot{m}$ value achievable with hydrogen was approximately 8 times higher than the $J^2/\dot{m}$ value achieved with argon for the same cylindrical thruster geometry.

Previous investigators[9,32,33] have proposed that the maximum stable operating value of $J^2/\dot{m}$ varies inversely with the square root of the propellant molecular weight, a trend which has apparently been reproduced in the numerical experiments presented here. Based on the simulation results presented above, Equation 1 was modified to incorporate the effect of propellant molecular weight on stable cylindrical self-field thruster operation:

$$\frac{J^2}{\dot{m}} \le \frac{6.25\times10^6}{Rc}\left(\frac{Lc}{La}\right)\left(\frac{M_{Ar}}{M_{pr}}\right)^{0.57} * \left[5 - \left(\frac{La}{Lc}\right) + 4\left(\frac{10*Rc-Ra}{2.5}\right)\right] \frac{A^2\text{-s}}{kg} \qquad (3)$$

where M_{Ar} represents the molecular weight of argon (39.95 amu) and M_{pr} represents the molecular weight of the propellant of choice (6.94 amu for lithium and 1.00 amu for the fully dissociated hydrogen modeled in this study). A better fit to the numerical results was obtained using an exponent of 0.57 rather than 0.5 for the molecular weight ratio, a distinction which should be clarified through refined modeling and/or additional experiments. The modified stability equation, subject to the geometric constraints associated with Equation 1, provides a simple analytic method to determine the maximum stable $J^2/\dot{m}$ value for cylindrical, self-field MPD thrusters operated with a variety of propellants.

The electromagnetic thrust may be expressed analytically as:[34]

$$T_{EM} = \frac{\mu_0}{4\pi}\left[\ln\left(\frac{Ra}{Rc}\right) + \alpha\right] J^2 \quad (N) \qquad (4)$$

where $0\le\alpha\le3/4$, depending on the assumed current distribution model. For $\alpha=0$, Equation 4 predicts an electromagnetic thrust of 1.0 N for the chosen geometry at 2500 A, independent of the propellant species. The value of the electromagnetic thrust calculated by the LeRC code for this geometry is 1.0 ± 0.01 N over the full range of simulated conditions and propellants, lending confidence to the accuracy of the numerical simulations and confirming that the electromagnetic thrust contribution is independent of the propellant species. The total thrust predictions shown in Figure 9 indicate that thermal acceleration processes contribute significantly to the total thrust, particularly for the lighter propellant species at lower $J^2/\dot{m}$ values. The ratio of thermal to electromagnetic thrust declines with decreasing mass flow rate (increasing $J^2/\dot{m}$), but the thermal component remains significant over the full range of simulated operating conditions.

The specific impulse, shown in Figure 10, increases as expected with increasing $J^2/\dot{m}$, reaching a value slightly in excess of 11,000 s for predicted stable thruster operation with hydrogen. An interesting feature of the graph is that the maximum stable I_{sp} value achieved with argon, 1300 s at $J^2/\dot{m}=5\times10^{10}$ A^2-s/kg, is approximately equal to the I_{sp} value of lithium, 1370 s, at the same $J^2/\dot{m}$ value. In turn, the maximum stable I_{sp} value achievable with lithium, 4340 s at $J^2/\dot{m}=1.75\times10^{11}$ A^2-s/kg, is nearly equal to the I_{sp} value of the thruster operated with hydrogen, 4500 s, at the same operating condition. As noted earlier, the thrust and associated specific impulse are primarily a function of electromagnetic acceleration processes at the highest achievable values of $J^2/\dot{m}$ for each propellant. The electromagnetic acceleration is independent of the propellant molecular weight (Equation 4), and as $J^2/\dot{m}$ is increased the specific impulse values for the various propellants should approach the same curve, as seen in the figure. The differences in the thrust and specific impulse values for the various propellants at a given $J^2/\dot{m}$ value are due to the additional thermal acceleration processes, which diminish in importance as the value of $J^2/\dot{m}$ is increased.

Figure 11 displays the predicted plasma potential for the thruster operated with the three propellants. The plasma potentials increase with increasing $J^2/\dot{m}$, and increase as a function of propellant molecular weight for given $J^2/\dot{m}$ values. The larger magnitudes displayed for the higher molecular weight propellants are due to the lower plasma temperatures associated with the heavier propellants at a given $J^2/\dot{m}$ value. The lower temperatures are reflected in lower plasma conductivity values, which produce higher electric fields for a given discharge current density.[17,18] The

plasma voltage is calculated by numerically integrating the radial electric field from cathode to anode, yielding higher plasma voltages for the higher molecular weight propellants.

The plasma potentials can be used to estimate the power deposited into the plasma, which can then be compared with the thrust power to determine the thruster flow efficiency:

$$\eta_f = \frac{T^2}{2\,\dot{m}\,V_{pl}\,J} \qquad (5)$$

where T denotes thrust, P_{pl} is the power deposited into the plasma, V_{pl} is the plasma fall voltage, and J is the discharge current. The total thruster efficiency will be significantly lower than the calculated flow efficiency, primarily because of power lost to the thruster electrodes. Nevertheless, the trends in flow efficiency may serve to identify regimes of potentially more efficient thruster operation. The flow efficiency as a function of $J^2/\dot{m}$ is plotted in Figure 12 for the three propellant species. The higher molecular weight propellants are limited by the combination of higher plasma potentials and lower total thrust values to flow efficiencies significantly lower than the thruster flow efficiencies associated with lower molecular weight propellants. The highest flow efficiencies are obtained at low $J^2/\dot{m}$ values with hydrogen, where the plasma potential is lowest and the total thrust is enhanced by a large thermal contribution. The flow efficiency associated with argon modestly increases with increasing $J^2/\dot{m}$, while the flow efficiency associated with lithium remains fairly constant with increasing $J^2/\dot{m}$ up to their respective maximum stable operating conditions. The flow efficiency associated with hydrogen rapidly falls with increasing $J^2/\dot{m}$, approaching a constant value of 0.6 as $J^2/\dot{m}$ continues to increase.

The flow efficiency results may be interpreted with the help of Figures 9 and 11. For argon, the thrust decreases slightly over the range of stable operating conditions, the plasma potential increases by roughly a factor of two, and the mass flow rate decreases by a factor of three over the range of stable $J^2/\dot{m}$ values (Table 1). From Equation 5, the expected net result is a slight increase in the flow efficiency for argon, as observed in Figure 12. For lithium, a more rapid decrease in thrust, a slower increase in the plasma potential, and a continual decline in the mass flow rate combine to produce a fairly flat efficiency profile. For hydrogen, the thrust drops rapidly as $J^2/\dot{m}$ is increased, then begins to level off at higher $J^2/\dot{m}$ values. Because the thrust is squared in the definition of flow efficiency, the large drop in the thrust combined with the increasing plasma potentials and decreasing mass flow rates result in a rapid initial drop in the flow efficiency, which then asymptotes at higher $J^2/\dot{m}$ values as the thrust approaches a constant value.

The flow efficiency results suggest that higher thruster efficiencies might be achieved in a given thruster geometry using low molecular weight propellants, in general agreement with experimental results.[5] However, the flow efficiency calculations do not include electrode processes, which are known to play an important role in thruster power deposition and subsequently in the total thruster efficiency.[17,18] The importance of electrode effects can be estimated from Figures 4 and 6, which show predicted plasma voltages and measured total voltages for the Princeton University full-scale benchmark thruster operated with argon and hydrogen propellants, respectively. The predicted plasma voltages are typically 2 to 3 times lower than the measured discharge voltages in each figure, and the corresponding flow efficiencies would be significantly higher than the actual thruster efficiencies of interest to the experimentalist or mission designer. Without an electrode model, the total power deposition and associated thruster efficiency cannot be accurately simulated. As noted throughout this study, an electrode model must be developed to further enhance the predictive capabilities of present MPD thruster simulations.

The two-temperature model assumed full propellant dissociation and ionization over the range of simulated $J^2/\dot{m}$ values, and Figure 13 may be used to gauge the validity of this approximation for the various propellant species. The total power deposited in the plasma (P_p) is obtained by multiplying the plasma potential and thruster discharge current, and represents the total available power for plasma heating, dissociation, ionization, and acceleration. To estimate whether the available plasma power is sufficient for full propellant dissociation and ionization, the calculated available power is divided by the sum of the calculated thrust power ($T^2/2\dot{m}$) and the power required for full propellant dissociation and ionization, given by:

$$P_{dis}+P_{ion} = \frac{(X_{dis}(eV) + 2*X_{ion}(eV))(1.6\times10^{-19}\,J/eV)(\dot{m})}{M_{pr}(amu)\,(1.6726\times10^{-27}\,kg)} \qquad (6)$$

where M_{pr} is the propellant molecular weight (amu), X_{dis} is the propellant dissociation potential (eV), and X_{ion} is the propellant ionization potential (eV), multiplied by a factor of two to account for each dissociated atom. Neither radiative nor convective heat transfer from the plasma to the simulated constant temperature thruster walls were modeled, and have been neglected in this preliminary power balance estimate. The ratio of available to required power, presented in Figure 13, indicates that the assumption of full ionization is approximately valid for argon over the full range of stable operating conditions, and may be valid for lithium at all but the lowest $J^2/\dot{m}$ value. However, there is insufficient power in the plasma to support the approximation of fully ionized hydrogen for most of the $J^2/\dot{m}$ values considered. Because the classical plasma transport coefficients used in the study remain approximately valid even at low ionization fractions,[26] the exceptionally poor assumption of fully ionized hydrogen is not expected to significantly change the thrust and plasma voltage predictions. However, the results do indicate that a proper evaluation of low molecular weight propellants should be undertaken with a numerical simulation incorporating non-equilibrium ionization models. This more detailed evaluation is left for a later numerical investigation.

Analytic Performance Estimates

The modified stability equation developed in the last section is useful for determining the maximum stable $J^2/\dot{m}$ values for a range of cylindrical self-field thruster geometries and a variety of propellant species. The maximum $J^2/\dot{m}$ values are associated with thruster operating regimes in which electromagnetic body forces provide a substantial fraction of the plasma acceleration, with thrust values approximately given by Equation 4. The corresponding values of maximum achievable specific impulse can be estimated from the relation:[24]

$$I_{sp} = \frac{\mu_0}{4\pi}\left[\ln\left(\frac{Ra}{Rc}\right)\right]\frac{J^2}{\dot{m}g} \quad (s) \qquad (7)$$

where g is the acceleration due to gravity (9.8 m/s^2) and μ_0 is the permeability of free space ($4\pi \times 10^{-7}$ H/m). However, because thermal acceleration processes have not been included, the total thrust and the associated specific impulse will be significantly underpredicted at low $J^2/\dot{m}$ values for all propellants, and will remain inaccurate at high $J^2/\dot{m}$ values for low molecular weight propellants.

Reported performance measurements for several cylindrical self-field MPD thrusters, operated over a range of discharge currents and mass flow rates, were used to formulate an empirical expression which might better approximate the total thrust and specific impulse. The total measured thrust was divided by the calculated electromagnetic thrust corresponding to Equation 4, and the results were plotted as a function of $J^2/\dot{m}$. A curve fitting routine was used to provide a simple analytic relation between the total thrust and the more easily calculated electromagnetic thrust. Figure 14 displays the results for several thrusters operated with argon, and Figure 15 displays the results for the FSBT and MY-I thrusters operated with hydrogen. Because limited experimental data were available for hydrogen, the numerical simulation results presented earlier were also included in the plot. No experimental data were available for lithium, and Figure 16 shows a curve fit corresponding solely to the numerical results presented in this report.

For argon, the experimental data could be accurately modeled with a curve fit of the form:

$$T_{(Ar)} = T_{EM}\left(1 + \frac{10^{10}}{J^2/\dot{m}}\right) \quad (N) \qquad (8)$$

Although more scatter was apparent in the hydrogen results, the data could be adequately modeled with a curve fit of the form:

$$T_{(H2)} = T_{EM}\left(1.5 + \frac{3\times10^{10}}{J^2/\dot{m}}\right) \quad (N) \qquad (9)$$

Based on the numerical results presented for lithium, it is estimated that a good fit to cylindrical self-field thruster performance with lithium propellant can be obtained using:

$$T_{(Li)} = T_{EM}\left(1.43 + \frac{1.4\times10^{10}}{J^2/\dot{m}}\right) \quad (N) \qquad (10)$$

The analytic expressions for each of the propellants can be combined into a single expression relating total thrust to calculated electromagnetic thrust as a function of propellant molecular weight and J^2/m:

$$T = T_{EM}\ [(1.52 - 0.013 \times M_{pr}) + (33.12 - 3.19 \times M_{pr} + 0.065 \times M_{pr}^2) \times 10^9/(J^2/\dot{m})]\ (N) \quad (11)$$

where M_{pr} denotes the propellant molecular weight in amu. The specific impulse is readily derived from the total thrust estimate using Equation 7. Although some scatter exists between the analytic expressions and experimental thrust values, the analytic predictions obtained with Equations 8-11 are typically within 20% of the measured total thrust values.

To test the general form of the total thrust equation, a comparison was performed between available experimental thrust data for the MY-1 thruster operated with ammonia[31] and the total thrust predicted by Equation 11. The results are presented in Figure 17. At $J^2/\dot{m}$ values below approximately 3×10^{10} A^2-s/kg, the thrust predicted by Equation 11 significantly underpredicts the measured thrust, indicating that for multispecies propellants the simple thrust equation does not accurately account for thermal acceleration processes. At $J^2/\dot{m} = 3 \times 10^{10}$ A^2-s/kg the predicted thrust is roughly 25% lower than the measured thrust. For $J^2/\dot{m}$ values above 3×10^{10} A^2-s/kg, the total predicted thrust becomes progressively more accurate, indicating that Equation 11 may still be of use for multispecies propellants at $J^2/\dot{m}$ values of interest. Thrust values for other less complex propellants, such as helium or pure nitrogen, could not be found in the open literature with sufficiently detailed information concerning thruster geometry and operating conditions to allow additional comparisons between experimental data and analytical predictions. Based on the results presented for argon, lithium, and hydrogen, it is expected that the general form of the total thrust equation will provide sufficiently accurate predictions for monopropellants over most operating conditions.

IV. SELF-FIELD MPDT DESIGN ALGORITHM

MPD thruster design has typically progressed through the proven if costly method of experimental trial and error. Numerical simulations have been developed which can accurately predict global thruster performance,[17-19,35-38] but without adequate computer resources the codes may require an excessive amount of time to survey the parameter spaces of interest. The combination of Equation 3, which predicts the maximum stable operating value of $J^2/\dot{m}$ for a range of cylindrical self-field thruster geometries and propellant atomic weights, and Equation 11, which yields a refined estimate for the total thrust and corresponding specific impulse as a function of $J^2/\dot{m}$, provides a useful new technique to estimate the performance of cylindrical, self-field MPD thrusters operated with a variety of propellants. Although not applicable to flared electrode designs or applied-field thrusters, the set of simple analytic equations presented above can be used to identify the cylindrical, self-field MPD thruster geometries most likely to meet required mission performance goals, reducing the set of detailed numerical simulations and experimental evaluations which must be performed.

The results outlined above suggest the following simple algorithm to estimate the thrust and specific impulse of cylindrical, self-field MPD thrusters. For a given discharge current, the cathode is sized to limit the required thermionic emission current density to values of approximately 20 A/cm^2, providing sufficient cathode lifetimes for missions of interest. Using this estimate for the minimum cathode surface area, Equation 3 can be iterated over a constrained range of cylindrical geometries to provide maximum stable $J^2/\dot{m}$ operating values. Previous simulations[18,19] indicate that optimum performance is obtained with short electrodes of nearly equal length, which reduces the number of geometries to be evaluated. The required mass flow rates can be obtained from the stable $J^2/\dot{m}$ values and the assumed discharge current. The electromagnetic thrust, Equation 4, may be evaluated for each stable geometry, and Equation 11 may then be used to better estimate the total thrust and related specific impulse. It should be remarked that, lacking a model for the total discharge voltage, no prediction can be made of the total thruster efficiency, which is equally important in the design of mission-competitive MPD thrusters. The ability to predict total discharge voltages for a variety of thruster geometries over a range of operating conditions must await further analytical and numerical developments.

Example.

Consider the design of a low power, cylindrical, self-field MPD thruster which is to be operated at a steady-state discharge current of 750 A. The presumed power is approximately 20 kW, which can be provided by solar photovoltaic arrays. The assumed power implies the thruster discharge voltage is limited to approximately 25 V, which is not unreasonable at the given discharge current.[39] The presumed specific impulse is 3000-5000 s for the

hypothetical mission of interest, perhaps an orbital transfer maneuver.

The cathode emission current density is limited to 20 A/cm^2, yielding a cylindrical cathode surface area of 37.5 cm^2 for long-life thermionic emission. Equation 3 is iterated over a range of cylindrical electrode geometries which satisfy both the minimum cathode surface area constraint and the geometric constraints associated with the validity of the equation: $5 \leq Rc/Ra \leq 10$, $1 \leq La/Ra \leq 5$, and $La \approx Lc$, where Rc, Lc, Ra, and La are the cathode radius, cathode length, anode radius, and anode length, respectively. The results indicate that a thruster geometry with a cathode radius of 1 cm, anode radius of 5 cm, and equal electrode lengths of 6 cm provides the highest stable J^2/m values for argon, subject to the constraints placed on the equation. The same geometry will provide maximum stable values of $J^2/\dot{m}$ for all propellants, though the magnitudes of $J^2/\dot{m}$ will be affected by the choice of propellant. The predicted maximum stable values of $J^2/\dot{m}$ are 7.4×10^{10} A^2-s/kg for argon, 1.2×10^{11} A^2-s/kg for ammonia, 2.0×10^{11} A^2-s/kg for lithium, and 6.0×10^{11} A^2-s/kg for hydrogen. The electromagnetic thrust, calculated from Equation 4, is 9×10^{-2} N for all propellants. The thrust due to propellant injection is a small fraction of the total thrust for low mass flow rates, and is neglected in the following results.

Equation 11 is used to predict the total thrust as a function of $J^2/\dot{m}$ for each propellant, up to their respective maximum stable $J^2/\dot{m}$ values. Given a constant discharge current of 750 A, the required mass flow rate is calculated for each value of $J^2/\dot{m}$. The associated specific impulse is then derived from the predicted total thrust and calculated mass flow rate according to Equation 7. The results are presented in Figures 18 and 19, which display the predicted specific impulse as a function of $J^2/\dot{m}$ for the various propellants. A minimum $J^2/\dot{m}$ value of 5.0×10^{10} A^{2}s-kg was assumed for ammonia, to remove uncertainties in the thermal thrust contributions associated with multispecies propellant predictions at low $J^2/\dot{m}$ values. For the given thruster geometry, neither argon nor ammonia were able to provide the minimum required specific impulse prescribed for the mission. Both lithium and hydrogen were able to provide specific impulse values in the range of interest, with hydrogen exceeding the mission requirements at high $J^2/\dot{m}$ values. Spacecraft contamination issues[5,23] might preclude the use of lithium, a condensable propellant, leading to hydrogen as the propellant of choice.

As noted earlier, the analysis cannot predict the thruster discharge voltage and total thruster efficiency. As a rough estimate, for a total discharge power on the order of 20 kW, Equation 5 indicates thruster efficiencies below 20% in the I_{sp} range of interest. Thruster efficiencies have been shown to improve with increasing discharge power,[5,28,29] typically exceeding 40% at power levels of a few megawatts. Although megawatt power sources for space applications are not available, megawatt power levels can be achieved in pulsed systems using available solar arrays coupled with capacitive storage and discharge systems.[40] The iterative procedure outlined above could thus be repeated for higher pulsed discharge currents corresponding to high peak power levels, until the cylindrical, self-field thruster design satisfies required values for estimated I_{sp} and efficiency. The preliminary design can then be further optimized with more sophisticated numerical simulations, leading to experimental testing and verification.

V. Concluding Remarks

A two-dimensional, two-temperature, single fluid magnetohydro-dynamics code was used to predict cylindrical self-field MPD thruster performance for a variety of propellants, assuming full propellant dissociation and ionization. Comparisons with the Princeton University full-scale benchmark thruster (FSBT) were performed for argon and hydrogen propellants, and comparisons were made with the Osaka University MY-I thruster operated with hydrogen. The model accurately predicted thrust and reproduced voltage-current trends for the FSBT operated with argon for $J^2/\dot{m}$ values below onset. The model accurately predicted thrust and reproduced I-V trends for the FSBT operated with hydrogen up to $J^2/\dot{m}$ values of 1.4×10^{11} A^2-s/kg. but underpredicted thrust at higher $J^2/\dot{m}$ values and did not converge for $J^2/\dot{m}$ values exceeding 2.2×10^{11} A^2-s/kg. Although the discrepancy may be due to the simplified model approximations, the experimentally measured discharge voltage displayed significant oscillations over the range of $J^2/\dot{m}$ values, indicating that the thruster may not have been operating stably with hydrogen. In addition, the observed erosion of insulator material may have contributed to the measured thrust at the higher discharge currents. Experimental FSBT thruster efficiencies with hydrogen were approximately 50% for $J^2/\dot{m}$ values near 3.2×10^{11} A^2-s/kg, and approached 70% for $J^2/\dot{m}$ values in excess of 4×10^{11} A^2-s/kg. However, the

maximum $J^2/\dot{m}$ value predicted by the numerical simulation for stable FSBT operation with hydrogen indicates a maximum thruster efficiency of around 20%, suggesting that higher efficiencies may have been purchased at the expense of thruster erosion and subsequent mass entrainment. The code accurately predicted thrust for the MY-1 thruster operated with hydrogen for $J^2/\dot{m}$ values approaching 2.1×10^{11} A^2-s/kg, but underpredicted the thrust at higher values by roughly 20%. As with the benchmark thruster, the thrust discrepancy at the high discharge currents could be an artifact of the simplified code approximations, or could result from the entrainment of eroded thruster material. These results reiterate the need to establish the role of thruster erosion and mass entrainment in thrusters operated at the low mass flow rates associated with low molecular weight propellants.

Although not entirely satisfactory, the code predictions were deemed sufficiently accurate for a preliminary study of propellant species effects in a cylindrical, self-field MPD thruster. A constant discharge current of 2500 A was assumed, and mass flow rates were adjusted to increase $J^2/\dot{m}$ values. Fully-ionized argon, lithium, and hydrogen propellants were modeled. Based on numerical convergence criteria, a thruster stability equation relating maximum stable $J^2/\dot{m}$ values to thruster geometry and propellant species was determined. The equation, which had been extensively validated for argon, indicated that stable $J^2/\dot{m}$ values scale as the inverse of the propellant molecular weight to the 0.57 power, in rough agreement with limited experimental data which indicate scaling as the inverse square root of propellant molecular weight.

Comparisons of measured total thrust and calculated electromagnetic thrust values were performed for a variety of cylindrical, self-field thrusters operated with various propellants. A set of curves were generated relating the total thrust to the electromagnetic thrust as a function of $J^2/\dot{m}$ and propellant species. A general equation was determined which can be used to predict the total thrust of cylindrical, self-field MPD thrusters as a function of the electromagnetic thrust, propellant species, and $J^2/\dot{m}$ operating value. An example was presented to illustrate the design of a low power MPD thruster based on a simple design algorithm which incorporates the stability and total thrust equations. Although total discharge voltage and corresponding thruster efficiencies cannot be predicted, the algorithm provides a useful tool to predict MPD thruster specific impulse for various propellants. Combined with estimates for the total discharge power, the design algorithm may be used to evaluate cylindrical self-field MPD thruster performance prior to more detailed numerical evaluations and experimental tests.

Acknowledgements

The author thanks the Department of Mechanical and Aerospace Engineering, Princeton University, for providing preliminary FSBT hydrogen performance data.

References

[1]Deininger, W. D. and Nock, K. T., "A Review of Electric Propulsion Spacecraft System Concepts", AIAA 90-2553, July 1990.

[2]Toki, K., Shimizu, Y., and Kuriki, K., "Application of MPD Thruster Systems to Interplanetary Missions", J. Prop. and Power, 2 (6), Nov.-Dec. 1986, pp. 508-512.

[3]Gilland, J. H., Myers, R. M., and Patterson, M. J., "Multi-megawatt Electric Propulsion System Design Considerations" AIAA 90-2552, July 1990.

[4]Sovey, J. S. and Mantenieks, M. A., "Performance and Lifetime Assessment of MPD Arc Thruster technology", AIAA 88-3211, July 1988.

[5]Myers, R. M., Mantenieks, M. A., and LaPointe, M. R., "MPD Thruster Technology", AIAA 91-3568, Sept. 1991; also NASA TM- 105242, Sept. 1991.

[6]Myers, R. M., "Applied-Field MPD Thruster Geometry Effects", AIAA 91-2342, June 1991.

[7]Martinez-Sanchez, M., "Structure of Self-Field Accelerated Plasma Flows", J. Prop. and Power, 7 (1), Jan.-Feb. 1991, pp. 56-64.

[8]Kunii, Y., Shimuzu, Y., and Kuriki, K., "Current Distribution in a Quasisteady MPD Arcjet with Various Anode Geometries", AIAA Journal, 22 (6), June 1984, pp. 750-751.

[9]Hugel, H., "Effect of Self-Magnetic Forces on the Anode Mechanism of a High Current Discharge", IEEE Transactions on Plasma Science, PS-4 (4), Dec. 1980, pp. 437-442.

[10]Subramaniam, V. V. and Lawless, J. L., "Onset in Magnetoplasmadynamic Thrusters with Finite-Rate Ionization", J. Prop. and Power, 4 (6), Nov.-Dec. 1988, pp. 526-532.

[11]Lawless, J. L. and Subramaniam, V. V., "Theory of Onset in Magnetoplasmadynamic Thrusters", J. Prop. and Power, 3 (2), Mar.- Apr. 1987, pp. 121-127.

[12]Wagner, H.P., Auweter-Kurtz, M., Roesgen, T., Messerschmid, E., and Kaeppeler, H. J., "Gradient Driven Instabilities in Stationary MPD Thruster FLows", AIAA 90-2603, July 1990.

[13]Smith, J. M., "Electrothermal Instability -An Explanation of the MPD Thruster Rotating Spoke Phenomena", AIAA 69-231, May 1969.

[14]Choueiri, E. Y., Electron-Ion Streaming Instabilities of an Electromagnetically Accelerated Plasma, Ph.D. Dissertation, Dept. of Mechanical and Aerospace Engineering, Princeton University, Princeton, NJ, October 1991.

[15]Tilley, D. L., An Investigation of Microinstabilities in a kW Level Self-Fleld MPD Thruster, M.S. Thesis, Dept. of Mechanical and Aerospace Engineering, Princeton University, Princeton, NJ, October 1991.

[16]Mantenieks, M. A. and Myers, R. M.,, "100-kW Class Applied-Field MPD Thruster Component Wear", NASA TM-106023, January 1993.

[17]LaPointe, M. R., "Numerical Simulation of Self-Field MPD Thrusters", AIAA 91-2341, June 1991; also NASA CR-187168, August 1991.

[18]LaPointe, M. R., "Numerical Simulation of Geometric Scale Effects in Cylindrical Self-Field MPD Thrusters", AIAA 92-3297, July 1992; also NASA CR-189224, August 1992.

[19]LaPointe, M. R., "Numerical Study of Cathode Emission Constraints on Cylindrical Self-Field MPD Thruster Performance", Tenth Symposium on Space Nuclear Power and Propulsion, M. El-Genk and M. Hoover (eds.), Albuquerque, NM, 1993, pp. 1447-1458.

[20]Preble, J. C., Onset in Magnetoplasmadynamic Thrusters: A Model of an Electrothermal Instability, M.S. Thesis, Dept. of Aeronautics and Astronautics, Massachusetts Institute of Technology, Cambridge, MA, May 1990.

[21]Schroff, A. M., Palluel, P., and Tonnerre, J. C., "Performance and Life Tests of Various Types of Impregnated Cathodes", Applications of Surface Science, 8 , North Holland Pub., 1981, pp. 36-49.

[22]Myers, R. M., Parkes, J. E., and Mantenieks, M. A., "Multimegawatt MPD Thruster Design Considerations", NASA TM 105405, January 1992.

[23]Polk, J. E. and Pivirotto, T. J., "Alkali Metal Propellants for MPD Thrusters", AIAA 91-3572.

[24]Randolph, T. M., von Jaskowsky, W.F., Kelly, A. J., and Jahn, R. G., "Measurement of Ionization Levels in the Interelectrode Region of an MPD Thruster", AIAA 92-3460, July 1992.

[25]Myers, R. M., Sverdrup Technology, Inc., NASA LeRC Group, Cleveland, OH, personal communication, 1993.

[26]Cambel, A. B., Plasma Physics and Magnetofluidmechanics, McGraw-Hill Pub., New York, NY, 1963, pp. 169-191.

[27]Gilland, J. H., "The Effect of Geometric Scale Upon MPD Thruster Behavior", M.S. Thesis, Dept. of Mechanical and AeroSpace Engineering, Princeton University, Princeton, NJ, March 1988.

[28]Miller, G. E. and Kelly, A. J., "Plasma Thruster Erosion Studies", in MAE 1776.38: Electric Propulsion Laboratory Progress Report, Dept. of Mechanical and Aerospace Engineering, Princeton University, Princeton, NJ, July-August 1992, pp. A5.1-A5.11.

[29]Kline, J. F. and Niederstrasser, C. G., "Control and Data Acquisition of Thrust and Efficiency Measurements for the Magnetoplasmadynamic (MPD) Thruster", in MAE 1776.40: Electric Propulsion Laboratory Progress Report, Dept. of Mechanical and Aerospace Engineering, Princeton University, Princeton, NJ, Nov.-Dec. 1992, pp. 1-41.

[30]Chouieri, E. Y., Dept. of Mechanical and Aerospace Engineering, Princeton University, Princeton, NJ, personal communication, 1993.

[31]Yoshikawa, T., Kagaya, Y., and Tahara, H., "Thrust Measurement of a Quasi-Steady MPD Arcjet", AIAA 85-2003.

[32]Merfeld, D. J., Kelly, A. J., and Jahn, R. J.,

"MPD Thruster Performance: Propellant Distribution and Species Effects", J. Prop. and Power, 2 (4), July-August 1986, pp. 317-322.

[33] Uematsu, K., Morimoto, S., and Kuriki, K., "MPD Thruster Performance with Various Propellants", J. Spacecraft and Rockets, 22 (4), July-August 1985, pp. 412-416.

[34]Jahn, R. G., Physics of Electric Propulsion, Chapter 8, McGraw-Hill Pub., New York, NY, 1968.

[35]Sleziona, P. C., Auweter-Kurtz, M., and Schrade, H. O., "Numerical Calculation of Nozzle Type and Cylindrical MPD Thrusters", AIAA 92-3296, July 1992.

[36]Mikellides, P. and Turchi, P., "Application of the MACH2 Code to Magnetoplasmadynamic Arcjets", AIAA 92-3740, July 1992.

[37]Niewood, E. H., An Explanation for Anode Voltage Drops in an MPD Thruster, Ph.D. Dissertation, Dept. of Aeronautics and Astronautics, Massachusetts Institute of Technology, Cambridge, MA, April 1993.

[38]Caldo, G., Choueiri, E. Y., Kelly, A. J., and Jahn, R. G., "Numerical Simulation of MPD Thruster Flows with Anomalous Transport", AIAA 92-3738, July 1992.

[39]Merke, W. D., Auweter-Kurtz, M., Habiger, H., Kurtz, H., and Schrade, H. O., "Nozzle Type MPD Thruster Experimental Investi-gations", IEPC 88-028, presented at the 20th International Electric Propulsion Conference, Garmisch-Partienkirchen, W. Germany, October 3-6, 1988.

[40]Myers, R. M., Domonkos, M., and Gilland, J. H., "Low Power Pulsed MPD Thruster System Analysis and Applications", AIAA 93-2391, June 1993.

[41]Wolff, M., Kelly, A. J., and Jahn, R. G., "A High Performance Magnetoplasmadynamic Thruster", IEPC 84-32, presented at the 17th International Electric Propulsion Conference, Tokyo, Japan, 1984.

$J^2/\dot{m}$	$\dot{m}$	THRUST (N)			I_{sp} (s)			V_p (V)			FLOW EFF.		
10^9 A^2-s/kg	10^{-6}kg/s	H_2	Li	Ar	H_2	Li	Ar	H_2	Li	Ar	H_2	Li	Ar
25	250	3.02	2.02	1.65	1235	826	675	7.35	8.95	10.2	0.98	0.37	0.22
50	125	2.19	1.68	1.58	1790	1370	1298	10.3	12.4	16.0	0.75	0.36	0.25
75	83	1.91	1.59	--	2350	1953	--	13.1	16.1	--	0.67	0.38	--
100	63	1.77	1.56	--	2870	2530	--	15.7	19.9	--	0.64	0.39	--
125	50	--	1.55	--	--	3160	--	--	24.0	--	--	0.40	--
150	42	1.62	1.53	--	3934	3730	--	20.7	27.5	--	0.61	0.41	--
175	36	--	1.53	--	--	4340	--	--	31.6	--	--	0.41	--
200	31	1.54	--	--	5057	--	--	25.5	--	--	0.60	--	--
250	25	1.49	--	--	6070	--	--	29.7	--	--	0.60	--	--
300	21	1.46	--	--	7080	--	--	33.8	--	--	0.60	--	--
350	18	1.43	--	--	8113	--	--	38.1	--	--	0.60	--	--
400	16	1.43	--	--	9322	--	--	42.4	--	--	0.61	--	--
450	14	1.40	--	--	10280	--	--	47.6	--	--	0.59	--	--
500	12.5	1.39	--	--	11360	--	--	52.9	--	--	0.59	--	--
550	--	--	--	--	--	--	--	--	--	--	--	--	--

Table 1. Thrust, specific impulse (I_{sp}), plasma voltage (V_p), and flow efficiency for a simulated 100-kW_e class cylindrical, self-field MPD thruster operated with hydrogen (H_2), lithium (Li), and argon (Ar) propellants at a constant discharge current of 2500 A.

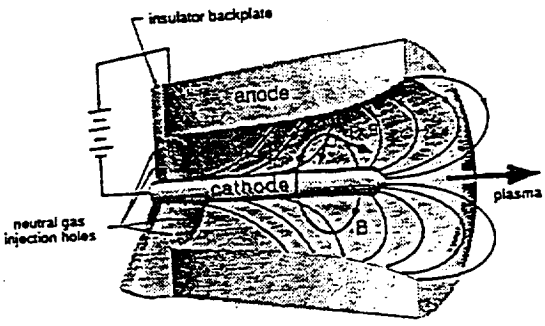

Figure 1. Generic MPD thruster schematic[14].

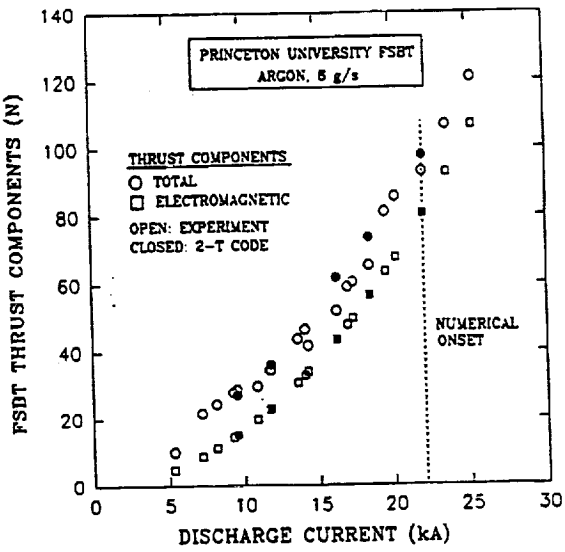

Figure 3. Comparison of measured[27,28] and predicted thrust for the Princeton University full-scale benchmark thruster operated with 6 g/s, argon. Dashed vertical line denotes onset of numerical oscillations.

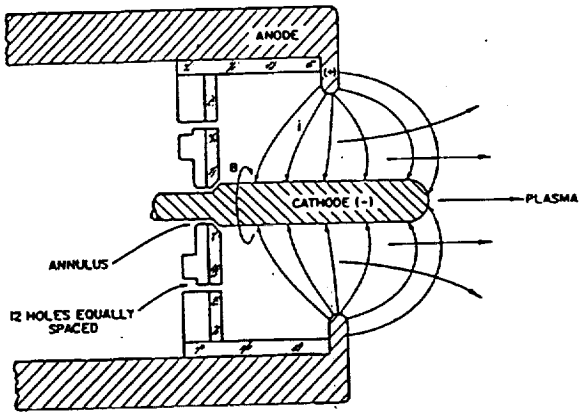

Figure 2. Princeton University full-scale benchmark thruster[26].

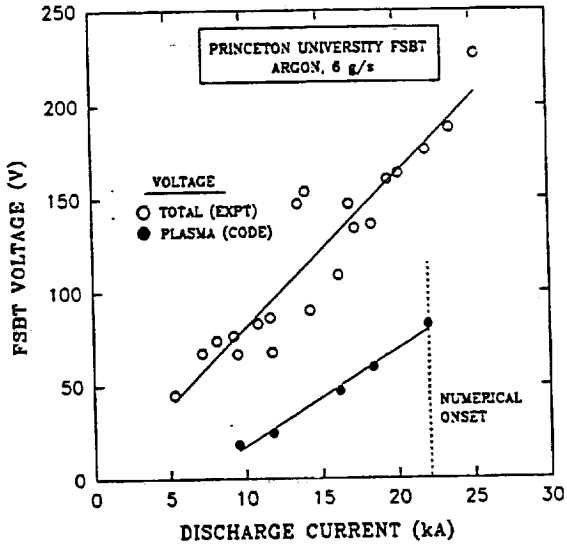

Figure 4. Comparison of measured total voltage[27,28] and predicted plasma voltage for the Princeton University full-scale benchmark thruster operated with 6 g/s, argon. Dashed vertical line denotes onset of numerical oscillations.

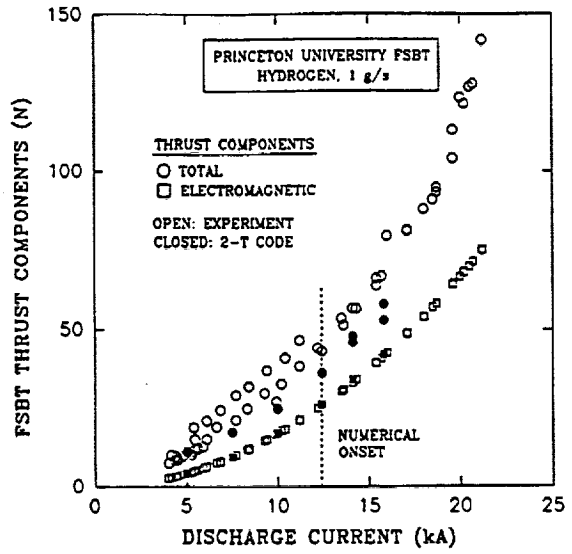

Figure 5. Comparison of measured[28,29] and predicted thrust for the Princeton University full-scale benchmark thruster operated with 1 g/s, hydrogen. Dashed vertical line denotes onset of numerical oscillations.

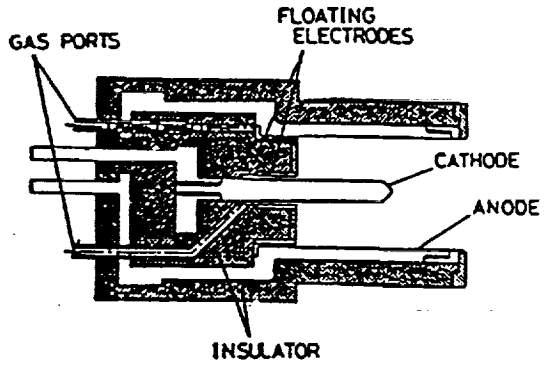

Figure 7. Osaka University MY-I thruster[31].

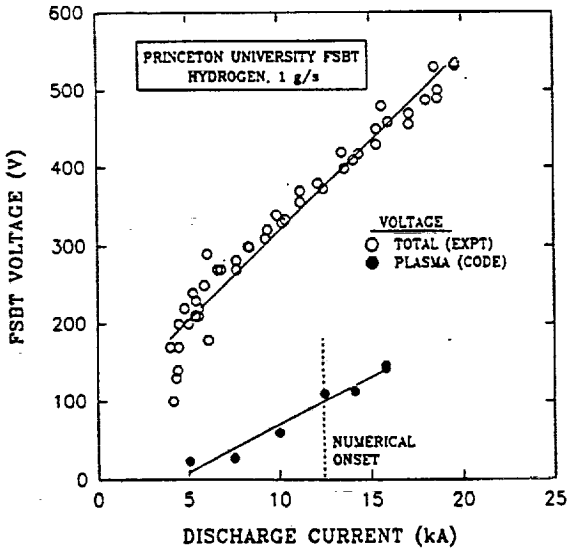

Figure 6. Comparison of measured total voltage[28,29] and predicted plasma voltage for the Princeton University full-scale benchmark thruster operated with 1 g/s, hydrogen. Dashed vertical line denotes onset of numerical oscillations.

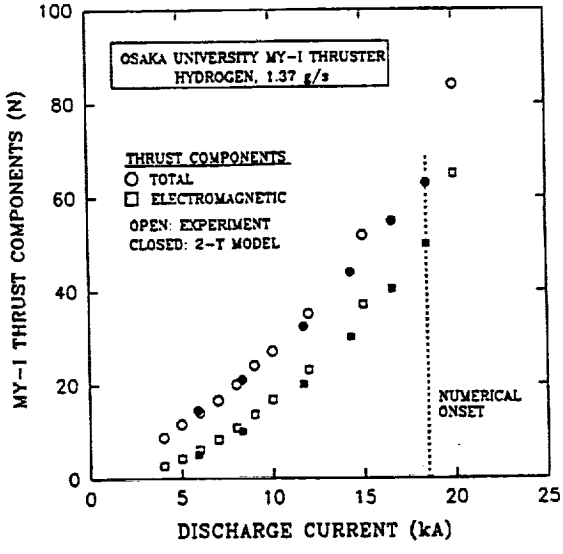

Figure 8. Comparison of measured[31] and predicted thrust for the Osaka University MY-I thruster operated with 1.37 g/s, hydrogen. Dashed vertical line denoted onset of numerical oscillations.

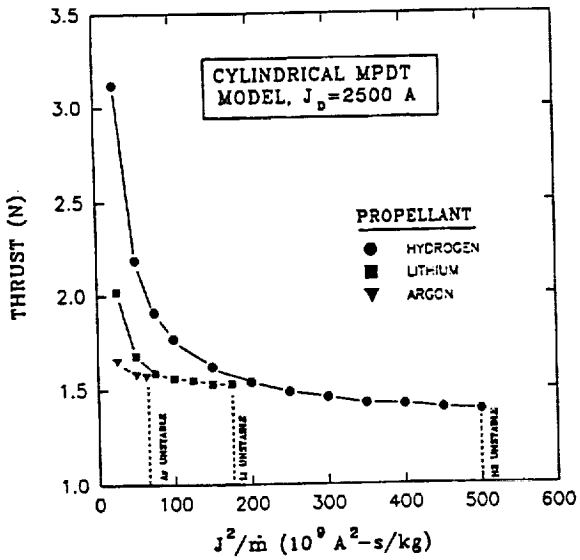

Figure 9. Predicted thrust for a simulated 100-kW class cylindrical, self-field MPD thruster operated with hydrogen, lithium, and argon propellants at a constant discharge current of 2500 A. Dashed vertical lines denote onset of numerical oscillations for each simulated propellant.

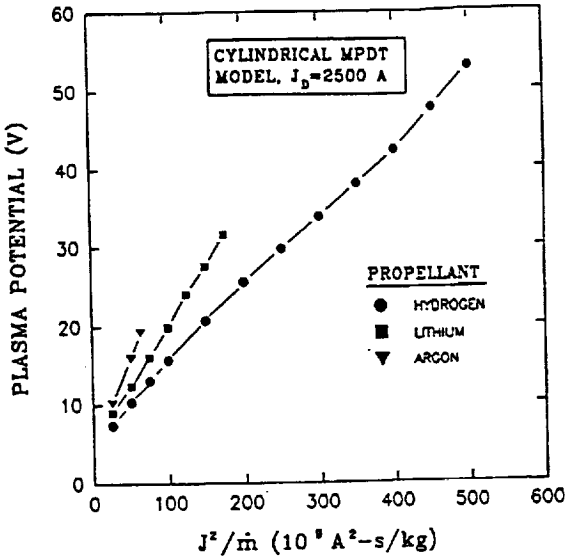

Figure 11. Predicted plasma potential for a simulated 100-kW class cylindrical, self-field MPD thruster operated with hydrogen, lithium, and argon propellants at a constant discharge current of 2500 A.

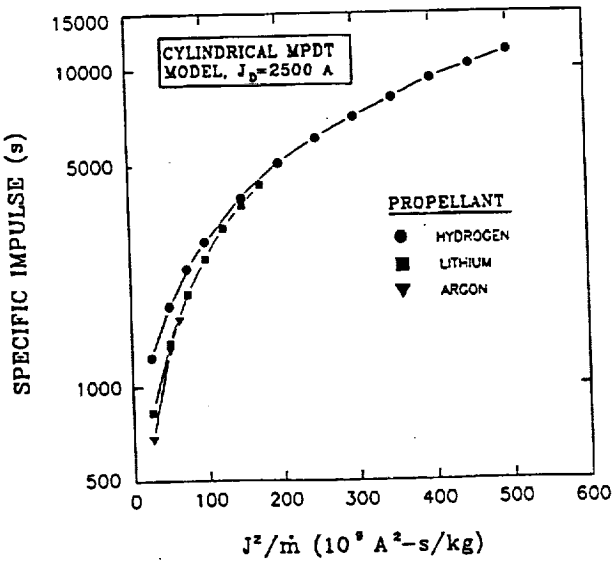

Figure 10. Predicted specific impulse for a simulated 100-kW class cylindrical, self-field MPD thruster operated with hydrogen, lithium, and argon propellants at a constant discharge current of 2500 A.

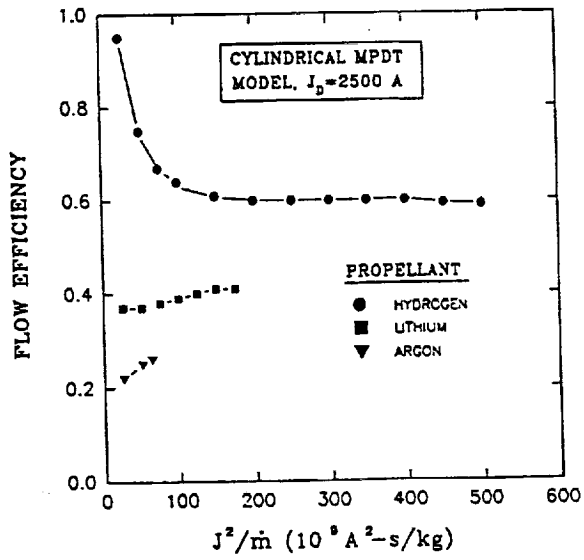

Figure 12. Predicted flow efficiency for a simulated 100-kW class cylindrical, self-field MPD thruster operated with hydrogen, lithium, and argon at a constant discharge current of 2500 A.

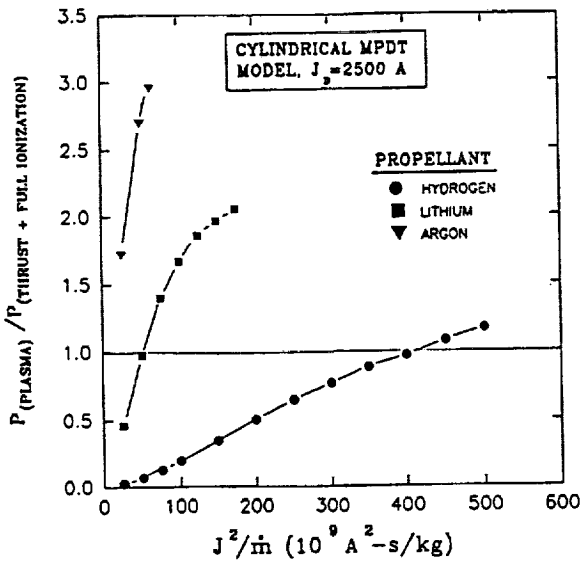

Figure 13. Ratio of the calculated power available in the plasma to the calculated power required for predicted thrust and full propellant ionization for a 100-kW class cylindrical, self-field MPD thruster operated with hydrogen, lithium, and argon at a constant discharge current of 2500 A.

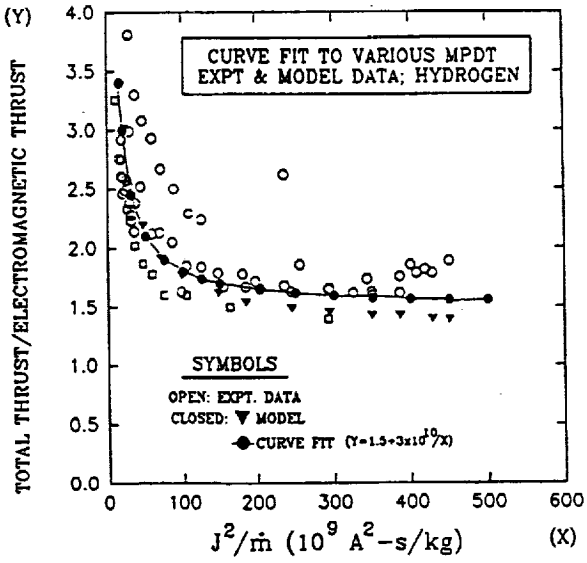

Figure 15. Curve fit to total/electromagnetic thrust as a function of J^2/m for the Princeton University full-scale benchmark thruster[28,29] operated at 1 g/s H_2 (o), the Osaka University MY-I thruster[31] operated at 1.37 g/s H_2 (□), and modeling predictions for a 100-kW class cylindrical, self-field MPD thruster operated with H_2 at a constant dicharge current of 2500 A (▼).

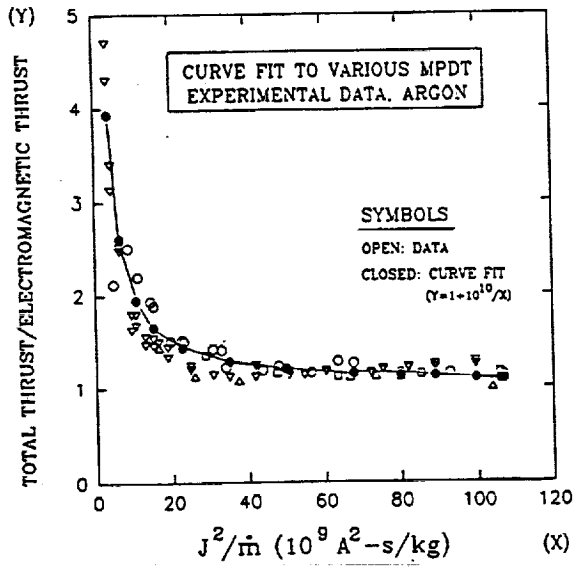

Figure 14. Curve fit to total/electromagnetic thrust as a function of $J^2/\dot{m}$ for the Princeton University full-scale benchmark thruster[27,28] operated at 6 g/s Ar (o) and 3 g/s Ar (□), the Princeton half-scale benchmark thruster[27] operated at 3 g/s Ar (▽), and the Princeton extended anode thruster[41] operated at 6 g/s Ar (△).

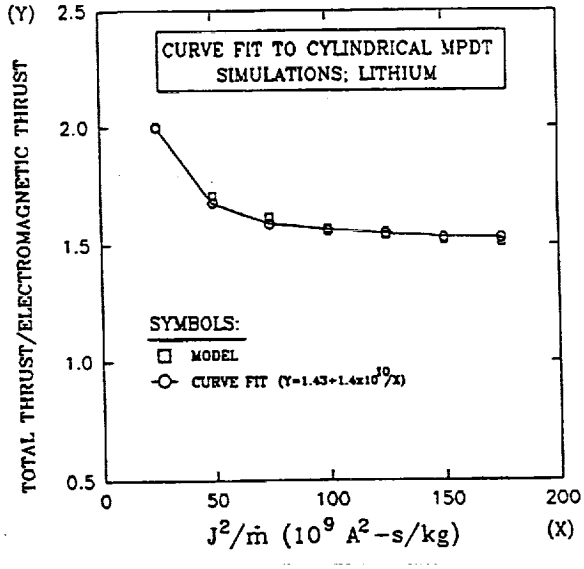

Figure 16. Curve fit to total/electromagnetic thrust as a function of $J^2/\dot{m}$ for a simulated 100-kW class cylindrical, self-field MPD thruster operated with Li.

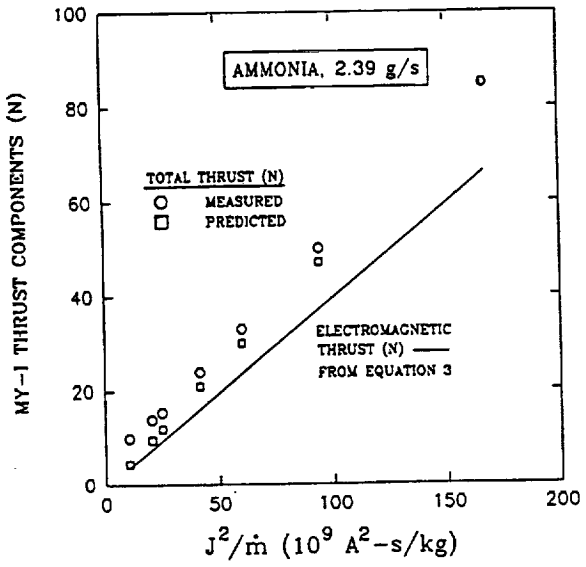

Figure 17. Comparison of predicted thrust using Equation 11 and measured total thrust for the Osaka University MY-I thruster[31] operated at 2.39 g/s, ammonia.

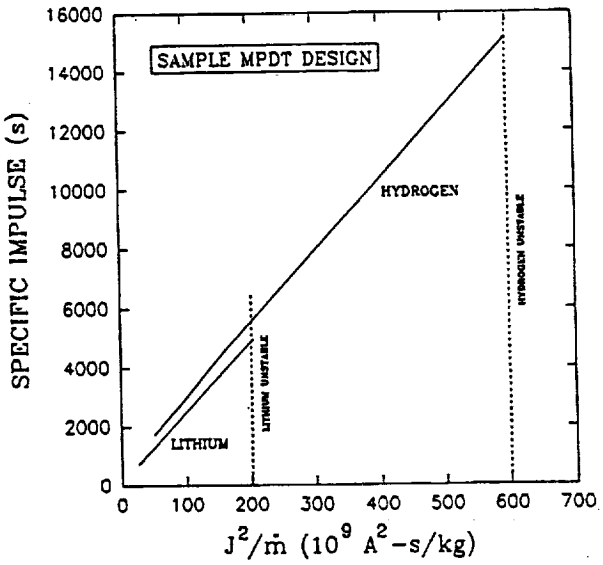

Figure 19. Predicted specific impulse with lithium and hydrogen for the example MPD thruster design. Dashed verical lines denote predicted limits of stable operation for each propellant.

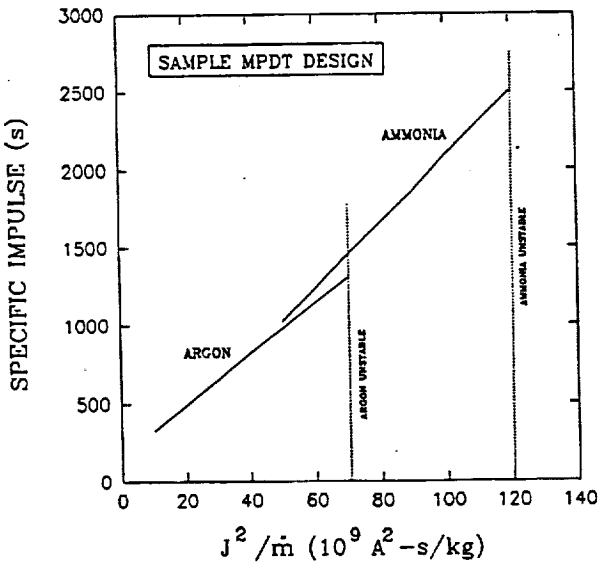

Figure 18. Predicted specific impulse with argon and ammonia for the example MPD thruster design. Dashed vertical lines denote predicted limits of stable operation for each propellant.

REPORT DOCUMENTATION PAGE

Form Approved
OMB No. 0704-0188

1. AGENCY USE ONLY (*Leave blank*)	2. REPORT DATE	3. REPORT TYPE AND DATES COVERED
	March 1994	Final Contractor Report

4. TITLE AND SUBTITLE
Numerical Simulation of Cylindrical, Self-Field MPD Thrusters With Multiple Propellants

5. FUNDING NUMBERS
WU–506–42–81
C–NAS3–25266

6. AUTHOR(S)
Michael R. LaPointe

7. PERFORMING ORGANIZATION NAME(S) AND ADDRESS(ES)
Sverdrup Technology, Inc.
Lewis Research Center Group
2001 Aerospace Parkway
Brook Park, Ohio 44142

8. PERFORMING ORGANIZATION REPORT NUMBER
E–8481

9. SPONSORING/MONITORING AGENCY NAME(S) AND ADDRESS(ES)
National Aeronautics and Space Administration
Lewis Research Center
Cleveland, Ohio 44135–3191

10. SPONSORING/MONITORING AGENCY REPORT NUMBER
NASA CR–194458

11. SUPPLEMENTARY NOTES
Prepared for the 23rd International Electric Propulsion Conference sponsored by the ASC, AIAA, DGLR, AIDAA, and JSASS, Seattle, Washington, September 13–16, 1993. Michael R. LaPointe presently at NYMA, Inc., Engineering Services Division, 2001 Aerospace Parkway, Brook Park, Ohio 44142. Project Manager, James S. Sovey, Space Propulsion Technology Division, organization code 5330, NASA Lewis Research Center, (216) 977–7454.

12a. DISTRIBUTION/AVAILABILITY STATEMENT
Unclassified - Unlimited
Subject Categories 20 and 64

12b. DISTRIBUTION CODE

13. ABSTRACT ***(Maximum 200 words)***

A two-dimensional, two-temperature, single fluid MHD code was used to predict the performance of cylindrical, self-field MPD thrusters operated with argon, lithium, and hydrogen propellants. A thruster stability equation was determined relating maximum stable $J^2/\dot{m}$ values to cylindrical thruster geometry and propellant species. The maximum value of $J^2/\dot{m}$ was found to scale as the inverse of the propellant molecular weight to the 0.57 power, in rough agreement with limited experimental data which scales as the inverse square root of the propellant molecular weight. A general equation which relates total thrust to electromagnetic thrust, propellant molecular weight, and $J^2/\dot{m}$ was determined using reported thrust values for argon and hydrogen and calculated thrust values for lithium. In addition to argon, lithium, and hydrogen, the equation accurately predicted thrust for ammonia at sufficiently high $J^2/\dot{m}$ values. A simple algorithm is suggested to aid in the preliminary design of cylindrical, self-field MPD thrusters. A brief example is presented to illustrate the use of the algorithm in the design of a low power MPD thruster.

14. SUBJECT TERMS	15. NUMBER OF PAGES
MPD; Electric propulsion; Numerical simulation	21
	16. PRICE CODE: A03

17. SECURITY CLASSIFICATION OF REPORT	18. SECURITY CLASSIFICATION OF THIS PAGE	19. SECURITY CLASSIFICATION OF ABSTRACT	20. LIMITATION OF ABSTRACT
Unclassified	Unclassified	Unclassified	